Inorganic Chemistry

ARTICLE

pubs.acs.org/IC

# Chirality and Diastereoselection of Δ/Λ-Configured Tetrahedral Zinc Complexes through Enantiopure Schiff Base Complexes: Combined Vibrational Circular Dichroism, Density Functional Theory, $^1$H NMR, and X-ray Structural Studies

Anne-Christine Chamayou,[†] Steffen Lüdeke,[*,‡] Volker Brecht,[‡] Teresa B. Freedman,[§] Laurence A. Nafie,[§] and Christoph Janiak[*,†,⊥]

[†]Institut für Anorganische und Analytische Chemie and [‡]Institut für Pharmazeutische Wissenschaften, Universität Freiburg, Albertstrasse 21, D-79104 Freiburg, Germany

[§]Department of Chemistry, Syracuse University, Syracuse, New York 13244-4100, United States

Supporting Information

**ABSTRACT:** The metal-centered Δ/Λ-chirality of four-coordinated, nonplanar Zn(A^B)$_2$ complexes is correlated to the chirality of the bidentate enantiopure (*R*)-A^B or (*S*)-A^B Schiff base building blocks [A^B = (*R*)- or (*S*)-*N*-(1-(4-*X*-phenyl)ethyl)salicylaldiminato-$\kappa^2$*N*,*O* with X = $OCH_3$, Cl, Br]. In the solid-state the (*R*) ligand chirality induces a Λ-M configuration and the (*S*) ligand chirality quantitatively gives the Δ-M configuration upon crystallization as deduced from X-ray single crystal studies. The diastereoselections of the pseudotetrahedral zinc-Schiff base complexes in $CDCl_3$ solution were investigated by $^1$H NMR and by vibrational circular dichroism (VCD) spectroscopy. The appearance of two signals for the Schiff-base −CH═N− imine proton in $^1$H NMR indicates an equilibrium of both Δ- and Λ-diastereomers with a diastereomeric ratio of roughly 20:80% for all three ligands. VCD proved to be very sensitive to the metal-centered Δ/Λ-chirality because of a characteristic band representing coupled vibrations of the two ligand's C═N stretch modes. The absolute configuration was assigned on the basis of agreement in sign with theoretical VCD spectra from Density Functional Theory calculations.

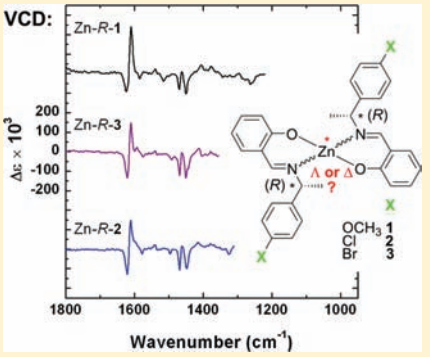


## INTRODUCTION

Since their very first application as catalysts in stereoselective synthesis[1] optically active transition metal complexes,[2,3] including chiral-at-metal complexes,[4] are of constant interest. Classical textbook examples of metal-centered chirality are pseudo-octahedral six-coordinate tris- or bis-chelate Δ/Λ-metal complexes. Here, the asymmetry is due to the arrangement of an achiral or chiral ligand A^A$^{(*)}$ around a metal M, leading to $D_3$ symmetry for Δ/Λ-M(A^A)$_3$ or $C_2$ symmetry for Δ/Λ-M(A^A)$_2$B$_2$, respectively.[2,5,6] Little attention, however, has been drawn on metal-centered chirality of four-coordinate metal complexes. It occurs in nonplanar systems with two asymmetrical chelate rings A^B rendering a complex M(A^B)$_2$ with $C_2$ symmetry. The metal-centered configuration can be described using the Δ/Λ-nomenclature originally introduced for trigonal complexes.[7] The chelate ring is interpreted as a segment of a helix or screw along the $C_2$ rotation axis (Scheme 1).[8−10]

There are continuous developments of optically active Schiff base (HSB*) ligands and their transition metal complexes[11] for applications as enantioselective catalysts,[12] compounds for second harmonic generation,[13] chiral magnetic metal clusters,[14] chiral fluorescent sensors,[15] as homochiral porous lamellar solids for enantioselective recognition and separation,[16] and dielectric materials.[17]

If the chelate ligand contains a single, configurationally stable stereogenic center, the *R*- or *S*-chirality of the ligand ((*R*)-A^B or (*S*)-A^B) and the Δ- or Λ-configuration at the metal center can give rise to four different stereoisomers, if enantiomerically pure ligands are combined with the metal atom: Λ-[M((*R*)-A^B)$_2$] and Δ-[M((*R*)-A^B)$_2$] or Λ-[M((*S*)-A^B)$_2$] and Δ-[M((*S*)-A^B)$_2$] (Scheme 2).

As a general rule, the diastereomeric ratio depends on the thermodynamics of stereochemical induction by the ligand. While this mechanism is well studied for octahedral[2,5,18] or five-coordinated complexes[19] relatively little activity has been invested in the diastereoselection of four-coordinate, asymmetric complexes. Here, the Δ- or Λ-configuration can interconvert through ligand exchange or rearrangement to a planar geometry. The kinetics of this process depend on the stability of metal−ligand interaction. Zinc ions are generally supposed to form weak interactions with ligand atoms. Nevertheless, they are

**Received:** May 6, 2011
**Published:** October 21, 2011

**Scheme 1. Enantiomeric Absolute Configurations of a Pseudotetrahedral, Nonplanar Bis-Chelate Complex Viewed down the $C_2$ Axis[a]**

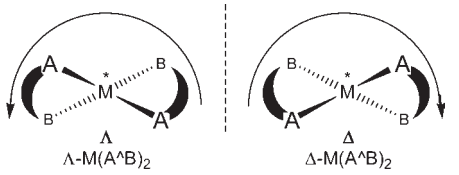


[a] Λ left-handed helicity, Δ right-handed helicity along principal $C_2$ axis (perpendicular to the paper plane). A and B convey the chelate ring asymmetry.[9]

**Scheme 2. Enantiomeric and Diastereomeric Δ/Λ-[M((*R*/*S*)-A^B)$_2$] Pairs[a]**

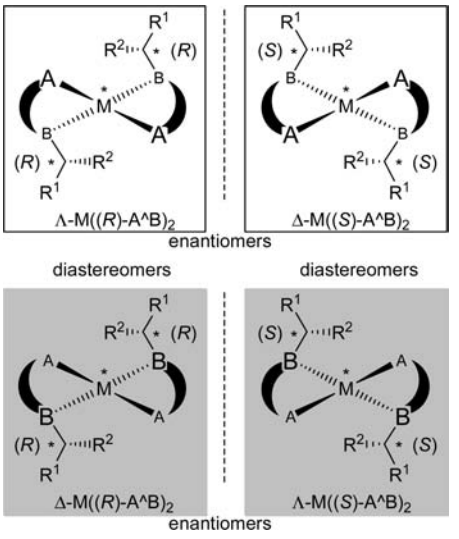


[a] The position of the *R*- or *S*-stereogenic center on the branched α-carbon of the B substituent is adapted to the present work (see Scheme 3) but could also reside in or on the A^B chelate handle. The priority for the *R*- or *S*-assignment should be B > R$^1$ > R$^2$. In the present work Λ-metal−(*R*)-ligand complexes and Δ-metal−(*S*)-ligand complexes in the white boxes are the major combination. The opposite and here minor Δ-metal−(*R*)-ligand complexes and Λ-metal−(*S*)-ligand combinations are underlined in gray (see Table 3).

highly abundant in biological systems, being essential for the functionalities of a number of metalloproteins, expressing both catalytic and structural roles.[20−22] In the cases of enzymes and zinc finger proteins, the cation is usually tetrahedrally coordinated[23] leading to a defined asymmetric geometry involving the zinc atom in their active site. This implies that a defined tetrahedral asymmetric structure can be established even with weak metal−ligand interactions, mediated by strong stereochemical induction by the ligand.

To study this issue one will have to be careful concerning the choice of method for determining both the absolute configuration and the diastereomeric composition. If a single crystal of sufficient size and quality is available, a straightforward method for determination of the metal-centered absolute configuration is single-crystal X-ray structural analysis.[24,25] The solid state structure, however, does not necessarily represent the geometry which is the thermodynamically most favorable one in solution or in the

**Scheme 3. Enantiopure (*R*)- or (*S*)-*N*-(1-(4-*X*-phenyl)ethyl)salicylaldimine Ligands and Major Δ/Λ-bis{(*R*)- or (*S*)-*N*-(1-(4-*X*-phenyl)ethyl)salicylaldiminato-κ$^2$*N*,*O*}zinc-(II) Complexes[a]**

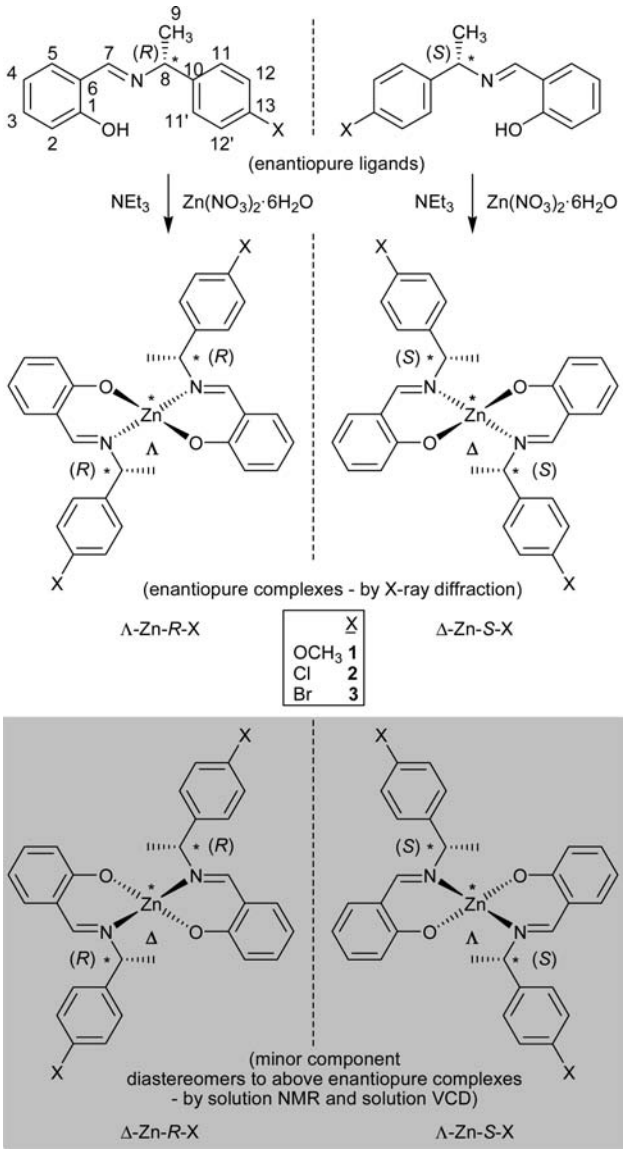


[a] The minor Δ-Zn−*R*-ligand complexes and Λ-Zn−*S*-ligand combinations are underlined in gray (see Table 3).

gas phase. During crystallization various parameters involving intermolecular contacts and lattice forces might become important. This might severely shift the equilibrium between Δ- and Λ-geometry at the metal ion, possibly even leading to inversion of the absolute configuration. Thus, no quantitative information about stereochemical induction can be drawn from the crystal structure.

To obtain reliable results about the Δ/Λ-equilibrium in solution in a noninvasive way, that is, avoiding any bias by molecular interactions with reagents, chromatography columns, and so forth, it is necessary to use a combination of spectroscopic methods. The equilibrium between two diastereomers can be easily studied using nuclear magnetic resonance (NMR). Integration of characteristic signals with different chemical shifts for

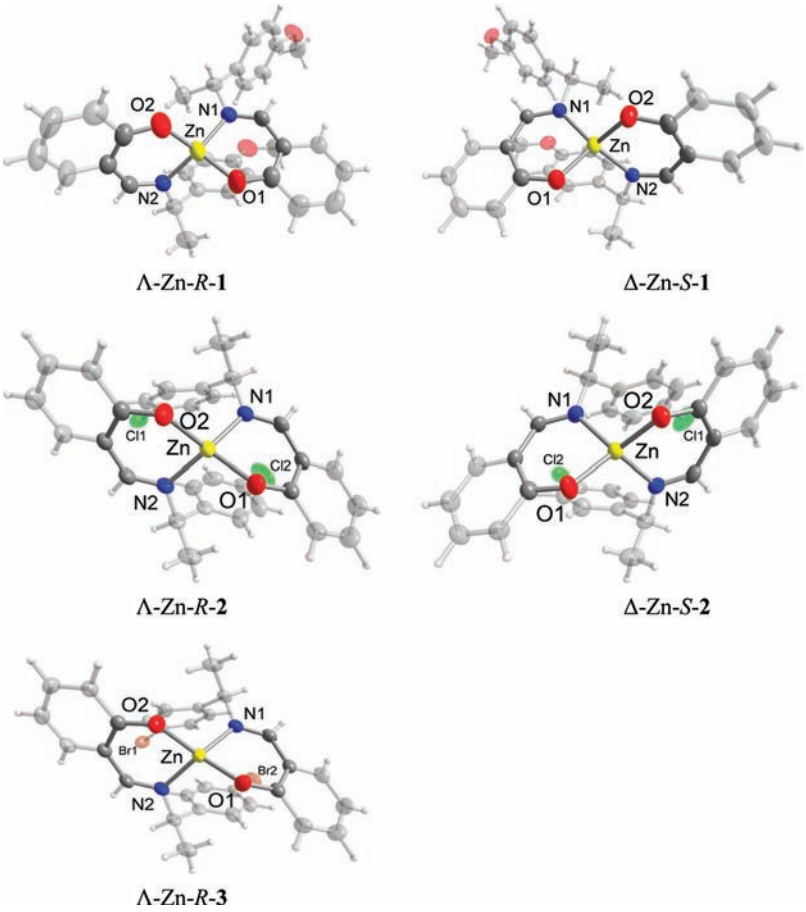


**Figure 1.** Thermal ellipsoid plots (50% probability) of the enantiomeric zinc complexes in a perspective, central projection to enhance the view of the Λ, left-handed helicity (left column) and Δ, right-handed helicity (right column) along the pseudo-$C_2$ axis (perpendicular to the paper plane). The two chelate rings are highlighted. Note that the thermal ellipsoids in the front appear larger than they really are because of the central projection. See Supporting Information, Figures S6−S10, for full atom numbering.

the Δ- and the Λ-diastereomer readily delivers the diastereomeric ratio. This approach, however, does not allow assignment of the absolute configuration of the excess (and the deficient) diastereomer which can be accomplished using chiroptical spectroscopy, in particular circular dichroism (CD).[26] Here, the difference absorbance of left minus right circularly polarized light is measured. Thus, the sign of the obtained bands is characteristic of the absolute configuration of the molecule. Electronic CD (ECD), which detects the difference absorbance of visible or UV-light, delivers good results for molecules with a chromophore with a transition dipole moment being coupled to a chirality element. For chiral complexes these could be either ligand transitions or d-d transitions of the metal ion.[27] Tetrahedrally coordinated zinc, which is only present as $d^{10}$ zinc(II) in biological complexes,[28] often does not exhibit characteristic bands in ECD. Thus, this method cannot provide sufficient information about metal−ligand bonding. Quasi-enantiomeric helical ligand chirality in pentacoordinate Zn complexes could, however, be assessed by the quasi-mirror images of the n→π* transition in ECD.[29] Vibrational CD (VCD) detects the coupling of vibrational modes to a chirality element and is therefore not subject to such limitations. Additionally, VCD samples the electronic ground state properties of a molecule. As a consequence, the assignment of absolute configuration by comparing experimental spectra to spectra from quantum-chemical calculations for VCD is obtainable at comparably low computational cost. This method is typically very reliable, which is because spectra are composed of many characteristic infrared bands corresponding to $3N - 6$ vibrational transitions. VCD is therefore a widely accepted tool for the determination of chiral configurations[30,31] and has recently also been applied for studies of the structure of chiral metal complexes.[32−34]

We describe here the solid-state structures and solution VCD and NMR studies of Δ/Λ-bis{(*R*)- or (*S*)-N-(1-(4-*X*-phenyl)ethyl)salicylaldiminato-$\kappa^2$*N,O*}zinc(II) complexes, synthesized from A^B asymmetric and enantiopure (*R*)- or (*S*)-salicylaldimine chelate ligands (Scheme 2 and Scheme 3). These pseudotetrahedral structures involving a chiral zinc ion serve as a model for studies on the diastereoselection of the Δ/Λ-metal configuration from the (*R*/*S*)-ligand chirality and on the equilibrium of the Δ/Λ-configuration in solution.

## RESULTS AND DISCUSSION

By refluxing $Zn(NO_3)_2 \cdot 6H_2O$ with the enantiopure (*R*)- or (*S*)-*N*-(1-(4-*X*-phenyl)ethyl)salicylaldimine Schiff bases shown in Scheme 3 and triethylamine (for deprotonation) in methanol, the bis{*N*-(1-(4-*X*-phenyl)ethyl)salicylaldiminato-$\kappa^2$*N,O*}zinc(II) complexes were obtained in the form of light-yellow crystals (Supporting Information, Figures S1−S5). The complexes were


dx.doi.org/10.1021/ic2009557 |*Inorg. Chem.* 2011, 50, 11363–11374

**Scheme 4. Assessment of Deviation between Tetrahedral and Square-Planar Geometry by the Dihedral Angle $\theta$ or the $\tau_{tet\text{-}sq}$ Index**

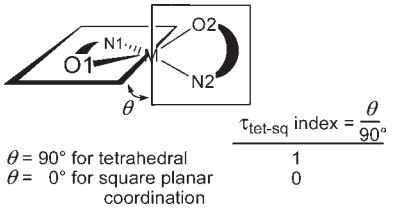


analyzed and characterized by elemental analysis, specific rotation, IR, NMR, their single-crystal X-ray structures, and solution VCD.

**Solid State Structural Studies.** The zinc atoms in the complexes synthesized here with the ligands **1**−**3** have a four-coordinate structure. The two *N,O*-bidentate Schiff base ligands form a distorted $N_2O_2$-tetrahedral coordination sphere around the zinc atom (Figure 1).

By considering the pseudo-$C_2$ axis passing through the center of the O1···O2 edge, the metal atom and the center of the N1···N2 edge, the absolute configuration Δ or Λ is determined (Scheme 1) and given as part of the compound designation (Figure 1). For a given (*R*) or (*S*) ligand chirality only one Δ or Λ configuration can be found as based on the absolute structure or Flack parameter of less than 0.07 (cf. Table 5).[25] Such a Flack parameter close to zero confirms the correct absolute structure and together with the other refinement parameter and with normal atom temperature factors and the absence of molecular disorder rules out that any significant amount of complexes with the opposite metal chirality, that is, a diastereomeric mixture, is present within one of the investigated crystals. We note that a single-crystal X-ray structure (based on only one crystal) would not rule out the possibility of a diastereomeric mixture of, for example, Δ-Zn-*R*-L and Λ-Zn-*R*-L forms with each Δ and Λ configuration crystallizing separately in an overall diastereomeric crystal mixture, akin to spontaneous resolution.[35] It can be noted that for the zinc compounds described here the Λ-Zn configuration correlates with the (*R*) ligand chirality (Λ-Zn-*R*-L) and the Δ-Zn configuration correlates with the (*S*) ligand chirality (Δ-Zn-*S*-L, Figure 1). The Δ or Λ configuration is induced diastereospecifically by the conformational preference of the chelate rings which results from the steric requirements of the substituents. The apparently more general preference for the Λ-M-*R*,*R* configuration in bis(salicylaldiminato)metal compounds is thought to be driven by the minimization of steric hindrance between the two ligands in the coordination sphere.[8,9,13]

Visual inspection of the molecular structures in Figure 1 already shows that the four-coordinated bis-chelate zinc complexes described here lie close to a tetrahedral configuration around the metal.

For a more quantitative assessment, the degree of distortion from tetrahedral or square planar can be expressed by the dihedral angle $\theta$ between the two planes formed by the donor atoms with the metal atom, that is, N1-M-O1 and N2-M-O2 (Table 2). This dihedral angle will be 90° for a tetrahedral geometry and 0° for a square planar geometry (not considering the imminent distortion induced by the chelate ring formation).[36] Furthermore, this angle $\theta$ can be normalized through division by 90° ($\theta$/90°) to give an index $\tau_{tet\text{-}sq}$ = 1.00 for tetrahedral and 0.00 for square planar geometry (Scheme 4).

**Table 1. Measure of Distortions from Tetrahedral or Square Planar Metal Geometry in the Bis{N-(1-(4-*X*-phenyl)-ethyl)salicylaldiminato-$\kappa^2$N,O}zinc(II) Complexes**

| *X* | compound designation | $\theta$/deg[a] | $\tau_{tet\text{-}sq} = \theta/90°$ | $\tau_4$[37, b] |
|---|---|---|---|---|
| -$OCH_3$ | Λ-Zn-*R*-**1** | 75.37(8) | 0.84 | 0.761 |
| | Δ-Zn-*S*-**1** | 75.0(7) | 0.83 | 0.760 |
| -Cl | Λ-Zn-*R*-**2** | 81.66(7) | 0.91 | 0.814 |
| | Δ-Zn-*S*-**2** | 81.77(9) | 0.91 | 0.816 |
| -Br | Λ-Zn-*R*-**3** | 82.31(8) | 0.91 | 0.821 |

[a] Calculated with Diamond.[39] [b] See Table 2 for the two largest angles $\alpha$ and $\beta$.

Also, a geometry index $\tau_4$ for four-coordinate complexes with $\tau_4 = [360° - (\alpha + \beta)]/141°$ has been proposed,[37] inspired by Addison and Reedijk's five-coordinate $\tau_5$ index,[38] with $\alpha$ and $\beta$ being the two largest angles in the four-coordinate species. The values of $\tau_4$ will range from 1.00 for a perfect tetrahedral geometry, since 360 − 2(109.5) = 141, to zero for a perfect square planar geometry, since 360 − 2(180) = 0. Intermediate structures, including trigonal pyramidal and seesaw, fall within the range of 0 to 1.00.[37] For two chelate ligands, as in the present bis-bidentate Schiff base complexes, it is, however, better to take the dihedral angle $\theta$ or its normalization index $\tau_{tet\text{-}sq} = \theta/90°$. The geometry index $\tau_4$ will not correctly assess a tetrahedral geometry because of the already imminent distortion induced by the chelate ring formation. With chelate ligands the two largest angles will inevitable be larger than 109.5°; hence, $\tau_4 < 1$, even if the dihedral planes are perfectly perpendicular. Both measures of distortion are listed in Table 1 and support the notion of a close to tetrahedral structure for zinc(II) complexes.

The Zn−O and Zn−N lengths and bond angles in the bis{*N*-(1-(4-*X*-phenyl)ethyl)salicylaldiminato-$\kappa^2$*N*,*O*}zinc(II) complexes are listed in Table 2 and are as expected.[8,40−44]

**NMR-Determination of Diastereomeric Ratio.** From X-ray studies of selected single crystals we can assume that a certain configuration at the ligand causes a quantitative induction of a certain configuration at the metal ion (diastereoselection) during the crystallization process of Zn-**1**, Zn-**2**, and Zn-**3**, respectively. Yet to what extent does this induction still hold when the crystalline complex is dissolved? To determine the diastereomeric ratio of Δ:Λ in solution we performed $^1$H NMR measurements in $CDCl_3$. For a quantitative evaluation we chose the imine proton at C-7 represented by a singlet above 8 ppm for each diastereomer. The assignment was performed by 2D-NMR methods (data and details are given in Supporting Information, Figure S11). The corresponding signals and integration results are given in Figure 2.

The appearance of two signals indicates that, different from the solid state, the solution in $CDCl_3$ allows for an equilibrium of both Δ- and Λ-diastereomers with a diastereomeric ratio of roughly 20:80% for all three Zn-*R* derivatives. This suggests that the substitution at the phenyl ring does not have a strong impact on the thermodynamic equilibrium. The kinetics for the Λ-to-Δ interconversion, however, seems to depend on the substituent. This is indicated by the different resolution of the respective signals, since a rate of about the same magnitude as the time resolution of the NMR experiment would lead to signal broadening. This is the case for Δ-Zn-*R*-**2** (chlorine, Figure 2a) and Δ-Zn-*R*-**3** (bromine, Figure 2c), where the substituents


dx.doi.org/10.1021/ic2009557 |*Inorg. Chem.* 2011, 50, 11363–11374

**Table 2. Bond Distances (Å) and Angles (deg) in the Zinc Complexes**

| | Λ-Zn-*R*-**1** | Δ-Zn-*S*-**1** | Λ-Zn-*R*-**2** | Δ-Zn-*S*-**2** | Λ-Zn-*R*-**3** |
|---|---|---|---|---|---|
| Zn−O1 | 1.928(2) | 1.906(2) | 1.918(2) | 1.917(3) | 1.924(2) |
| Zn−O2 | 1.934(2) | 1.923(2) | 1.915(2) | 1.920(3) | 1.920(3) |
| Zn−N1 | 2.004(2) | 2.019(2) | 2.018(2) | 2.023(3) | 2.026(3) |
| Zn−N2 | 2.007(2) | 2.036(2) | 2.021(2) | 2.025(3) | 2.028(3) |
| O1−Zn−O2 | 119.91(10) | 119.45(9) | 119.35(9) | 119.11(11) | 118.07(12) |
| O1−Zn−N1 | 96.47(9) | 96.63(8) | 94.60(9) | 94.92(12) | 94.46(11) |
| O1−Zn−N2 | 107.38(10) | 106.38(9) | 111.79(9) | 112.72(13) | 111.94(11) |
| O2−Zn−N1 | 107.16(10) | 106.95(9) | 112.77(10) | 111.63(13) | 112.84(12) |
| O2−Zn−N2 | 95.54(10) | 96.24(9) | 94.55(9) | 94.71(12) | 95.30(11) |
| N1−Zn−N2 | 132.72(11) | 133.39(10) | 125.94(10) | 125.83(13) | 126.14(13) |

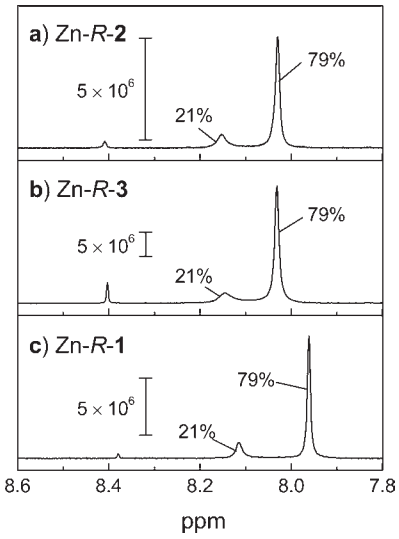


**Figure 2.** NMR signals around 8.1 ppm and 8.0 ppm account for the −CH═N− imine proton at C-7 of the Δ- and Λ-diastereomer of Zn-*R*-**1**, Zn-*R*-**2**, and Zn-*R*-**3**, respectively. The diastereomeric ratio (%) is from integration of the corresponding signals. The additional signal around 8.4 ppm corresponds to C-7 of the free ligand *R*-**1**, *R*-**2**, or *R*-**3**, respectively.

might allow for interconversion near the NMR time scale. Methoxy (Figure 2c), on the other hand, seems to retard interconversion between both diastereomers. This results into well resolved and separated singlets. An additional singlet around 8.4 ppm indicates presence of free ligand *R*-**1**, *R*-**2**, or *R*-**3**, respectively. This was proven by a "spike-in" experiment, where free ligand *R*-**2** was added to a sample of Zn-*R*-**2** (Figure 3a). The amount of free ligand depends on the amount of water being present in the sample. Presence of water leads to rapid hydrolysis of the complex as could be shown from a hydrolysis experiment where $D_2O$ was added to a solution of Zn-*R*-**2** in $CDCl_3$ (Figure 3b).

**Density Functional Theory (DFT) Calculations and Solution VCD Experiments.** The diastereomeric Δ:Λ- ratio of about 20:80% for all tested Zn-*R* complexes implies that the crystallization process had contributed to full asymmetric induction from the ligand in the solid phase, as suggested from single crystal X-ray crystallography. In solution, on the other hand, asymmetric induction might be decreased or even

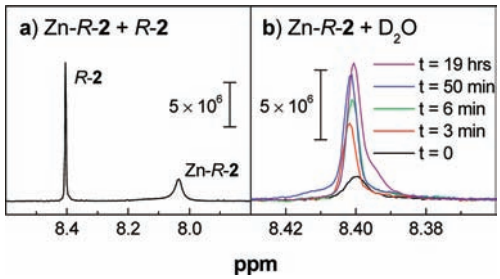


**Figure 3.** Signal at 8.4 ppm could be assigned to free ligand. The spike-in experiment (addition of free ligand *R*-**2** to a sample of Zn-*R*-**2**) leads to increase of the signal at 8.4 ppm (a). Presence of free ligand depends on presence of water in the solvent. Addition of $D_2O$ to a sample of Zn-*R*-**2** leads to rapid increase of the signal at 8.4 ppm because of hydrolysis of the complex (b).

inverted by Δ/Λ-interconversion through a planar intermediate. We addressed this question by VCD-based determination of the absolute configuration at the metal ion of the excess diastereomer in solution for Zn-**1**, Zn-**2**, and Zn-**3**. The chiral metal ion should have a strong influence on vibrational modes corresponding to coordinating ligand atoms. Hence, we expected VCD to be highly sensitive for the metal-centered asymmetry of chiral tetrahedral zinc complexes.

In view of the fact that contributions from both the Δ- and the Λ-species have to be taken into account to create a theoretical spectrum we calculated vibrational frequencies and IR and VCD intensities for both the Δ- and the Λ-diastereomer based on modeled geometries for the determination of the absolute configuration in solution. We chose Zn-*R*-**2** as a model for all three variants presented here, since the chlorine substituent appeared to require the lowest computational cost compared to bromine in Zn-*R*-**3** (more basis functions needed to approximate the atomic orbitals) and methoxy in Zn-*R*-**1** (9-fold number of conformers). Conformer models were created on the assumption of a rigid, quasi-tetrahedral core structure around the metal ion, as suggested from X-ray data (Figure 1) and represent different rotamers around the single bond between the nitrogen atom and C-8 of the ligand (Supporting Information, Figure S12). After a two-step conformational analysis (see the experimental section for details) three low-energy geometries of Zn-*R*-**2** (two conformers of Λ and one conformer of Δ) where chosen for DFT calculation of IR/VCD spectra, relative energies ($\Delta E$), and relative free energies ($\Delta G$) at the B3LYP level, using

**Table 3. Boltzmann Weights Based on Relative Energies ($\Delta E$) and Relative Free Energies ($\Delta G$), Respectively for Three Modeled Geometries of Zn-*R*-2**[a]

| geometry | $\Delta E$ (kJ·mol$^{-1}$) | Boltzmann weights (%) in respect to $\Delta E$ | $\Delta G$ (kJ·mol$^{-1}$) | Boltzmann weights (%) in respect to $\Delta G$ |
|---|---|---|---|---|
| Λ-Zn-*R*-**2** | | | | |
| conformer 1 | 0.74 | 39 | 0 | 45 |
| conformer 2 | 4.58 | 8 | 0.79 | 33 |
| Δ-Zn-*R*-**2** | 0 | 53 | 1.83 | 22 |

[a] Supporting Information, Figure S12. Parameters are calculated at the B3LYP level, using Ahlrichs VTZ basis set for zinc and 6-31+G(d,p) for carbon, hydrogen, nitrogen, oxygen, and chlorine.

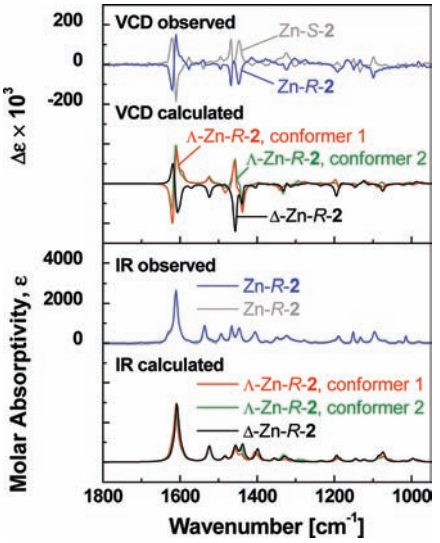


**Figure 4.** Experimental IR and VCD spectra of Zn-*R*-**2** (blue) and Zn-*S*-**2** (26 mM solution in $CDCl_3$) and calculated spectra corresponding to Λ-Zn-*R*-**2**, conformer 1 (red) and conformer 2 (green), respectively, and to Δ-Zn-*R*-**2** (black). While the calculated IR spectra are very similar for all three geometries, the VCD-spectrum of Δ-Zn-*R*-**2** is considerably different from those corresponding to the two Λ-conformers. The VCD band at 1622/1610 cm$^{-1}$ represents the in- and out-of-phase vibrations of the ligand's C═N stretch mode and can be used as a marker for the Δ/Λ-configuration: 1622(−)/1610(+) cm$^{-1}$ indicates Λ for Zn-*R*-**2**, the opposite sign indicates Δ for Zn-*S*-**2**.

Ahlrichs VTZ basis set on zinc[45] and 6-31+G(d,p) on all other atoms (GAUSSIAN[46]). The calculated values for $\Delta E$, $\Delta G$, and the Boltzmann weights both calculated in respect to $\Delta E$ and $\Delta G$ are given in Table 3. While the relative energies $\Delta E$ suggest about equal contributions of Δ and Λ, Boltzmann weights calculated in respect to $\Delta G$ (25 °C) lead to a diastereomeric ratio (Δ:Λ) of 22:78% being in very good agreement with NMR data (Figure 2). Conformer 1 of Λ, the most abundant geometry in respect to $\Delta G$, is most similar to the geometry from the crystal structure.

We compared the theoretical IR and VCD spectra calculated for conformers 1 and 2 of Λ-Zn-*R*-**2** and the single conformer of Δ-Zn-*R*-**2**, respectively, to IR and VCD spectra of Zn-*R*-**2** and Zn-*S*-**2** in solution (Figure 4). The experimental spectra of enantiomeric Zn-*R*-**2** (blue) and Zn-*S*-**2** (gray) appear as nearly perfect mirror images. The overall agreement between calculated spectra and the observed spectrum of Zn-*R*-**2** is better for the two

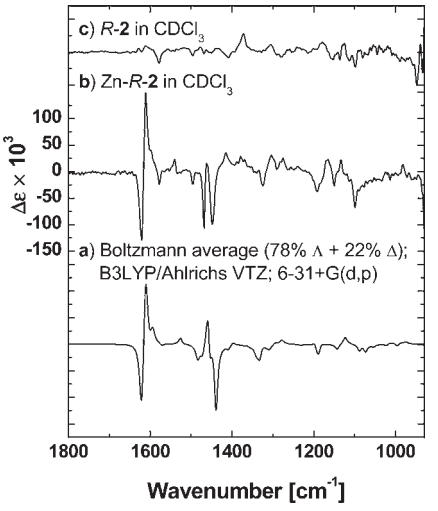


**Figure 5.** (a) Boltzmann average of theoretical spectra calculated for Λ-Zn-*R*-**2**, conformer 1 (45%), conformer 2 (35%), and for Δ-Zn-*R*-**2** (20%) leads to good overall agreement with the experimental spectrum (b). Contributions from the absolute configuration of the ligand are comparably small (c).

conformers of Λ-Zn-*R*-**2** (red, green) than for Δ-Zn-*R*-**2**. The agreement is particularly good for the VCD signal at 1622/1610 cm$^{-1}$ representing the in- and out-of-phase vibrations of the ligand's C═N stretch mode. The sign seems to coincide with the configuration at the metal ion: The calculated spectra of the Λ-conformers and the experimental spectrum of Zn-*R*-**2** both present a 1622(−)/1610(+) cm$^{-1}$ VCD-signal, allowing for the assignment of Λ-configuration at the metal ion to Zn-*R*-**2** and Δ-configuration to its enantiomer Zn-*S*-**2**. The latter exhibits the opposite 1622(+)/1610(−) cm$^{-1}$ VCD, agreeing with the corresponding signal in the spectrum calculated for diastereomeric Δ-Zn-*R*-**2** (black).

In the spectral region between 1500 and 1000 cm$^{-1}$ the experimental spectrum of Zn-*R*-**2** also shows spectral contributions from the Δ-species. This is in accordance with the results from NMR spectra in $CDCl_3$ solution and from gas phase calculations of $\Delta G$, suggesting a proportion of ∼20% Δ-Zn-*R*-**2** at room temperature. Figure 5a,b shows a theoretical spectrum representing the spectral contributions of the three modeled geometries of Zn-*R*-**2**, Boltzmann-averaged in respect to $\Delta G$, in comparison to the experimental spectrum of Zn-*R*-**2**. Deviations between calculated and observed spectra are most obvious for the band pattern around 1480 cm$^{-1}$. They might be due to slight over- or underestimation of the calculated frequencies leading to different band cancellation effects in the calculated spectrum and the measured spectrum. Nevertheless, on the basis of good overall agreement and of agreement in sign of the most prominent VCD signal at 1622/1610 cm$^{-1}$ it is evident that the excess diastereomer of Zn-*R*-**2** is Λ-configured at the metal ion. This means, that ∼80% of dissolved complex maintain the configuration which had been determined for solid Zn-*R*-**2** by single-crystal X-ray crystallography.

Interestingly, by evaluating the calculated spectra for Λ-Zn-*R*-2 and Δ-Zn-*R*-2, it becomes obvious that the configuration at the metal ion accounts for large difference signals in the VCD, while contributions originating from ligand chirality appear comparably small (Figure 5c). This could be explained by coupled vibrations due to a chiral arrangement of the vibrational

**Scheme 5. Relative Disposition of C═N Stretch Modes within the Geometries of Λ-Zn-*R*-2 (Conformer 1) and Δ-Zn-*R*-2[a]**

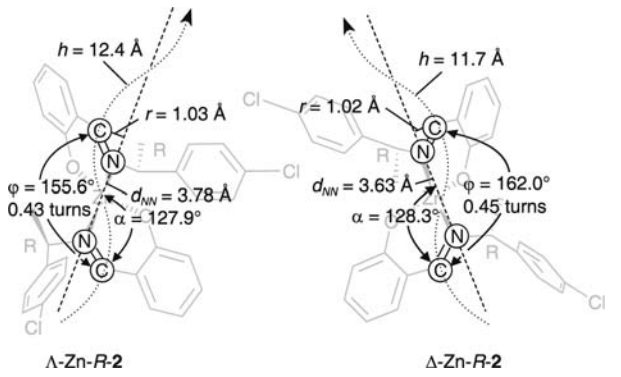


[a] The double bonded carbon atoms describe a helix around the N−N axis that is right-handed for the Λ-species and left-handed helix for the Δ-species. Helix radius ($r$) and pitch ($h$) can be calculated from atom distances ($d_{NN}$), the dihedral angle between the two C═N groups ($\varphi$), and the angle spanned between the C═N axis and the N−N axis ($\alpha$) which were taken from the optimized geometries from B3LYP/Ahlrichs VTZ, 6-31+G(d,p) calculations.

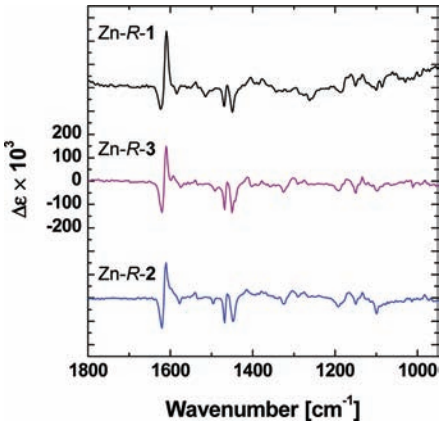


**Figure 6.** VCD spectrum is not significantly affected by different substituents at the aromatic side chain: Zn-*R*-**2**: -Cl; Zn-*R*-**3**: -Br; Zn-*R*-**1**: -$OCH_3$.

transition dipole vectors. The concept of coupled transition dipoles is well-known as exciton coupling in electronic CD and is a widely used tool for the assignment of the absolute configuration of molecules where two absorbing chromophores participate in a chiral system.[47−49] For VCD analogous examples for coupled vibrational transitions had recently been demonstrated for tris-(β-diketonato)metal(III) complexes[50] and mixed ruthenium 3-trifluoroacetylcamphorato/acetylacetonato complexes,[34] where large VCD signals originating from three helically arranged coordinated C═O stretch modes had been observed. Similarly, the relative disposition of C═N stretch modes in Λ-Zn-*R*-2 and Δ-Zn-*R*-2 may account for the large VCD in the complex spectra compared to the ligand spectrum (Figure 5). In the model structures, the dihedral angle (C−N−N−C) is 155.6° in Λ-Zn-*R*-2, and 162.0° in Δ-Zn-*R*-2, respectively. Taking into account the relative distance between the atoms, the double bonded carbons describe a right handed helix around the N−N axis with a radius of 1.0 Å and a pitch of 12.4 Å in Λ-Zn-*R*-2, and a left-handed helix with a

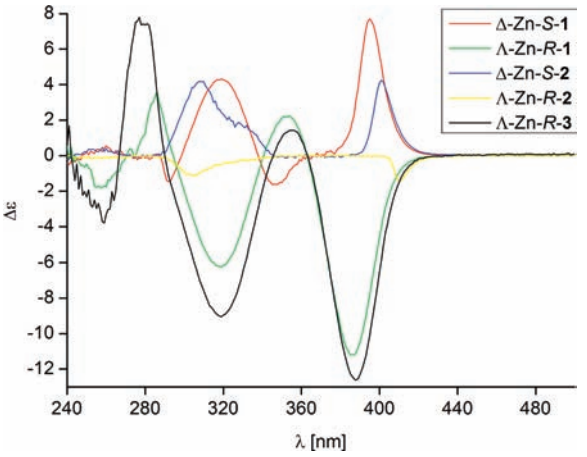


**Figure 7.** ECD spectra in $CHCl_3$ solution (concentrations in mol/L: Δ-Zn-*S*-**1** $4.0 \times 10^{-4}$, Λ-Zn-*R*-**1** $2.1 \times 10^{-4}$, Δ-Zn-*S*-**2** $7.7 \times 10^{-4}$, Λ-Zn-*R*-**2** $1.7 \times 10^{-3}$, Λ-Zn-*R*-**3** $1.3 \times 10^{-4}$).

radius of 1.0 Å and a pitch of 11.7 Å in Δ-Zn-*R*-2 (Scheme 5). Therefore, the VCD signal at 1622/1610 $cm^{-1}$ representing the in- and out-of-phase vibrations of both ligand's C═N stretch can be used as a sensitive probe for Δ/Λ-chirality in the tetrahedral complexes presented in this study.

The impact of different substituents at C-13 on the helical arrangement of the coupled vibrational modes should be negligible. Thus, the absolute configuration of the excess diastereomer of Zn-*R*-**1** and Zn-*R*-**3** as chloroform solutions can as well be assigned to the Λ-configuration on the basis of agreement in sign of the signal at 1622/1610 $cm^{-1}$ (Figure 6).

While the VCD spectra are dominated by coupled oscillator signals, in electronic CD ligand-specific transitions, being independent from metal-centered chirality, seem to result into similar intensities as complex-specific signals. The electronic CD spectra in solution show ligand bands in the region 240−440 nm (Figure 7). For $d^{10}$ Zn(II) there are no d-d transitions. Different from VCD the bands are significantly affected and, thus, shifted more by the substituents at the aromatic side chain. The spectra of enantiomers (Δ-Zn-*S*-**1** vs Λ-Zn-*R*-**1**, Δ-Zn-*S*-**2** vs Λ-Zn-*R*-**2**) do not appear as perfect mirror images, which could be explained by a different degree of hydrolysis as shown in Figure 3. As a consequence of the similar intensities of complex and ligand CD, electronic CD might be much more prone to frequency shifts from different amounts of free ligand than VCD. Nevertheless, the opposite sign of the transitions reflects the enantiomeric relationship between the complexes with ligand **1** and ligand **2**, respectively, supporting the results from VCD analysis.

## CONCLUSION

Using an optically active Schiff base (HSB*) ligand we have established a simple model for strong stereochemical induction on the metal-centered chirality of presumably weakly bound zinc(II). All three tested ligand derivates comprising different substituents (chlorine, bromine, methoxy) at the aromatic amine-moiety of the HSB* ligand led to identical induction in the solid state, determined by X-ray structural analysis. Solution analysis by NMR and VCD-based determination of the absolute configuration delivered virtually identical results for a diastereomeric ratio of ~20:80 for Δ-Zn-*R* versus Λ-Zn-*R* chloroform solutions at room temperature. These complexes might serve as an

**Table 4. Details of the yield, CHN analysis and characterization for the Δ/Λ-bis{(*R*)- or (*S*)-*N*-(1-(4-*X*-phenyl)ethyl)salicylaldiminato-$\kappa^2N,O$}zinc(II) complexes**

| X | compound designation | yield (g) (%) | %C, H, N - calc. - found | mp (°C) | $[\alpha]^{25}_{589}$ (°) (concentration, mg/mL) | IR ($cm^{-1}$) |
|---|---|---|---|---|---|---|
| -$OCH_3$ | Λ-Zn-*R*-**1** | 0.48 | 66.96, 5.62, 4.88 | 183 | −164.0 | 1611 (vs), 1534 (m), 1514 (m), 1466 (m), 1446 (m), 1404 (m), |
| | | 84 | 66.40, 5.77, 4.76 | | (4.6) | 1251 (m), 1147. (m), 1022. (m), 840 (m), 758 (m) |
| | Δ-Zn-*S*-**1** | 0.46 | 66.96, 5.62, 4.88 | 182 | +164.2 | 1610 (vs), 1526 (m), 1459 (s), 1403 (m), 1335 (m), 1299 (m), |
| | | 80 | 66.86, 5.71, 4.79 | | (8.1) | 1248 (s), 1186 (m), 1143 (m), 1021 (m), 836 (m), 754 (m) |
| -Cl | Λ-Zn-*R*-**2** | 0.44 | 61.82, 4.50, 4.81 | 163 | −221.0 | 1605 (vs), 1534 (s), 1451 (s), 1406 (s), 1313 (m), 1189 (m), 1142 (m), |
| | | 76 | 60.21, 4.57, 5.02 | | (1.0) | 1092 (s), 825 (s), 749 (vs), 599 (m), 541 (m), 511 (m), 479 (m), 438 (s) |
| | Δ-Zn-*S*-**2** | 0.45 | 61.82, 4.50, 4.81 | 160 | +221.4 | 1604 (vs), 1533 (m), 1447 (s), 1404 (m), 1309 (m), 1187 (m), 1143 (m), |
| | | 77 | 58.59, 4.81, 5.54 | | (2.6) | 1090 (s), 824 (s), 748 (vs), 599 (m), 540 (m), 512 (m), 479 (m), 436 (vs) |
| -Br | Λ-Zn-*R*-**3** | 0.52 | 53.64, 3.90, 4.17 | 179 | −228.5 | 1605 (vs), 1533 (s), 1451 (s), 1407 (s), 1312 (m), 1189 (m), 1142 (m), |
| | | 77 | 53.51, 3.90, 4.09 | | (10.4) | 1097 (m), 1068 (m), 821 (s), 749 (s), 524 (m), 433 (m), 406 (s) |

example for a dynamic diastereomeric equilibrium which is considerably shifted on one side by stereochemical induction from the ligand. Nevertheless, this equilibrium seems to be rather independent from the substituents at C-13. Further studies will have to address the question of ligand modifications leading to fine-tuning of this equilibrium.

## EXPERIMENTAL SECTION

Commercially available solvents, triethylamine, $Zn(NO_3)_2 \cdot 6H_2O$, and the enantiopure amines (from BASF AG, Ludwigshafen, Germany) (*R*)-1-(4-methoxyphenyl)ethylamine, (*S*)-1-(4-methoxyphenyl)ethylamine, (*R*)-1-(4-chlorophenyl)ethylamine, (*S*)-1-(4-chlorophenyl)ethylamine, (*R*)-1-(4-bromophenyl)ethylamine were used as received. Elemental analyses were performed on a VarioEL from Elementaranalysensysteme GmbH. Infrared spectra were recorded in the range 4000−400 $cm^{-1}$ on a Nicolet Magna 760 Spectrometer using a diamond orbit ATR unit. Polarimetric measurements were carried out with a Perkin-Elmer 341 polarimeter in $CHCl_3$ at 25 °C, and the specific optical rotation values of $[\alpha]^{25}_{589}$ were determined according to the literature.[51] Electronic circular dichroism (ECD) spectra were recorded on an Applied Biophysics Chirascan spectrometer with a 1 cm cell in $CHCl_3$.

$^1$H NMR, $^{13}$C NMR, and 2D spectra in $CDCl_3$ were recorded at 400 MHz on a Bruker DRX 400. $^1$H NMR spectra in $CD_3OD$ were recorded at 200 MHz on a Bruker Advance DPX 200. Chemical shifts in $CDCl_3$ refer to the solvent signal at 7.26 ppm for $^1$H NMR and 77.00 ppm for $^{13}$C NMR, respectively. Chemical shifts in $CD_3OD$ refer to the solvent signal at 3.31 ppm.

### Syntheses

**(*R*)- or (*S*)-*N*-(1-(4-*X*-phenyl)ethyl)salicylaldimines (1−3).**[52] A solution of salicylaldehyde (20 mmol, 2.11 mL) in methanol (10 mL) was stirred with two drops of conc. $H_2SO_4$ at room temperature for 10 min. After an equimolar amount of (*R*)- or (*S*)-*N*-(1-(4-*X*-phenyl)-ethylamine (20 mmol, 3 mL) was added the color changed to yellow, and the solution was refluxed for 5−6 h at 80 °C to give a yellow solution. The solvent was evaporated to half its volume in vacuum; then, the solution was allowed to evaporate slowly at room temperature. After 2−3 days, yellow bright crystals were obtained. See ref 52 for further details and characterization of *R*-**3**.

**(*S*)-*N*-(1-(4-methoxyphenyl)ethyl)salicylaldimine, *S*-1.** mp 70 °C. Yield: 5.19 g, 98.4%. $C_{16}H_{17}NO_2$ (255.32 g·$mol^{-1}$): calculated C 75.27, H 6.71, N 5.49; found C 74.03, H 6.73, N 5.42%. IR ($cm^{-1}$): 3076 (vw), 3047 (vw), 2994 (vw), 2977 (vw), 2960 (vw), 2935 (w), 2902 (vw), 2863 (vw), 2837 (w), 2719 (vw), 2656 (vw), 2536 (vw), 1623 (s), 1607 (s), 1579 (m), 1536 (w), 1511 (m), 1501 (m), 1461 (w), 1441 (m), 1415 (w), 1375 (m), 1338 (vw), 1317 (vw), 1303 (w), 1279 (s), 1244 (s), 1202 (w), 1180.9 (s), 1149.6 (m), 1126.0 (vw), 1114.7 (w), 1098.0 (m), 1067.7 (w), 1024.5 (s), 983.7 (vw), 972.3 (w), 941.4 (vw), 931.2 (vw), 914.0 (w), 884.6 (vw), 865.1 (w), 836.6 (s), 817.2 (m), 784.1 (w), 761.1 (vs), 718.3 (w), 675.1 (vw), 642.3 (w), 632.9 (w), 592.8 (w), 563.6 (w), 553.4 (vw), 536.1 (m), 521.2 (w), 481.1 (w), 435.7 (m). $^1$H NMR ($CD_3OD$, 200 MHz), δ/ppm (*J*/Hz) = 8.50 (s, 1H, H7), 7.35−7.25 (m, 4H, H3, H5, H11/11′), 6.95−6.80 (m, 4H, H2, H4, H12/12′), 4.59 (q, 1H, H8, *J* = 6.7), 3.77 (s, 3H, $OCH_3$), 1.59 (d, 3H, H9, *J* = 6.9) (see Scheme 3 for the NMR atom numbering). $[\alpha]^{25}_{589}$ (*c* = 11.9 mg/mL): +131.1°.

**(*R*)-*N*-(1-(4-methoxyphenyl)ethyl)salicylaldimine, *R*-1.** mp 68 °C. Yield: 5.22 g, 98%. $C_{16}H_{17}NO_2$ (255.32 g·$mol^{-1}$): calculated C 75.27, H 6.71, N 5.49; found C 75.01, H 6.71, N 5.31%. IR ($cm^{-1}$):3046.2 (vw), 2981.2 (vw), 2934.7 (vw), 2863.5 (vw), 2837.3 (w), 2362.5 (vw), 2338.2 (vw), 2058.0 (vw), 1966.7 (vw), 1021.2 (vw), 1896.2 (vw), 1622.8 (s), 1606.4 (s), 1579.9 (m), 1501.3 (s), 1458.4 (w), 1439.1 (w), 1373.1 (m), 1337.2 (vw), 1316.8 (vw), 1278.5 (vs), 1242.1 (vs), 1204.7 (w), 1180.4 (vs), 1149.0 (w), 1114.2 (w), 1096.9 (m), 1066.9 (w), 1023.2 (vs), 986.1 (vw), 971.9 (m), 913.0 (w), 881.6 (vw), 864.2 (w), 836.8 (vs), 817.8 (vw), 783.9 (w), 760.9 (vs), 717.3 (m), 639.5 (w), 591.7 (m), 561.8 (w), 535.1 (m), 521.2 (vw), 480.6 (w), 435.7 (m). $^1$H NMR ($CD_3OD$, 200 MHz), δ/ppm (*J*/Hz) = 8.49 (s, 1H, H7), 7.35−7.25 (m, 4H, H3, H5, H11/11′), 6.95−6.80 (m, 4H, H2, H4, H12/12′), 4.58 (q, 1H, H8, *J* = 6.7), 3.78 (s, 3H, $OCH_3$), 1.59 (d, 3H, H9, *J* = 6.9). (see Scheme 3 for the NMR numbering notation). $[\alpha]^{25}_{589}$ (*c* = 10.6 mg/mL): −131.3°.

**(*S*)-*N*-(1-(4-chlorophenyl)ethyl)salicylaldimine, *S*-2.** mp 46 °C. Yield: 5.77 g, 90%. $C_{15}H_{14}NOCl$ (259.74 g·$mol^{-1}$): calculated C 69.36, H 5.43, N 5.39; found C 68.77, H 5.36, N 5.41%. IR ($cm^{-1}$):3050.19 (w), 2972.11 (m), 2927.02 (m), 2885.77 (m), 1948.29 (w), 1901.37 (w), 1630.28 (vs), 1577.49 (s), 1491.51 (s), 1404.87 (s), 1278.32 (s), 1095.27 (s), 825.61 (vs), 758.19 (vs). $^1$H NMR ($CD_3OD$, 200 MHz), δ/ppm (*J*/Hz) = 8.54 (s, 1H, H7), 7.38−7.26 (m, 2H, H3, H5 and 4H, H11/11′, H12/12′), 6.92−6.83 (m, 2H, H2, H4), 4.61 (q, 1H, H8, *J* = 6.6), 1.59 (d, 3H, H9, *J* = 6.4). (see Scheme 3 for NMR atom numbering). $[\alpha]^{25}_{589}$ (*c* = 11.8 mg/mL): +140.9°.

**(*R*)-*N*-(1-(4-chlorophenyl)ethyl)salicylaldimine, *R*-2.** mp 38 °C. Yield: 11.51 g, 90%. $C_{15}H_{14}NOCl$ (259.74 g·$mol^{-1}$): calculated C 69.36, H 5.43, N 5.39; found C 69.21, H 5.58, N 5.38%. IR ($cm^{-1}$):2978.0 (vw), 2882.8 (vw), 1623.2 (s), 1575.9 (w), 1489.2 (m), 1451.6 (w), 1409.6 (w), 1376.6 (w), 1317.6 (vw), 1276.3 (m), 1204.0 (w), 1125.4 (w), 1086.3 (s), 1008.5 (w), 974.6 (w), 920.8 (w), 849.0 (vw), 824.6 (m), 749.7 (vs), 648.0 (w), 541.4 (m), 483.4 (w), 434.2 (m). $^1$H NMR ($CDCl_3$, 400 MHz), δ/ppm (*J*/Hz) = 13.35 (s, 1H, OH), 8.41 (s, 1H, H7), 7.35−7.28 (m, 1H (7.32, dd, H3) and 4H (H11/11′, H12/12′)), 7.25 (d, 1H, H5, *J* = 7.50), 6.97 (d, 1H, H2, *J* = 8.32), 6.89 (dd, 1H, H4, *J* = 7.46, 7.46), 4.52 (q, 1H, H8, *J* = 6.71), 1.61 (d, 3H,

**Table 5. Crystal Data and Structure Refinement for the Zinc Complexes**

| | Λ-Zn-*R*-**1** | Δ-Zn-*S*-**1** | Λ-Zn-*R*-**2** | Δ-Zn-*S*-**2** | Λ-Zn-*R*-**3** |
|---|---|---|---|---|---|
| empirical formula | $C_{32}H_{32}ZnN_2O_4$ | $C_{32}H_{32}ZnN_2O_4$ | $C_{30}H_{26}Cl_2ZnN_2O_2$ | $C_{30}H_{26}Cl_2ZnN_2O_2$ | $C_{30}H_{26}Br_2ZnN_2O_2$ |
| $M$/g·mol$^{-1}$ | 573.97 | 573.97 | 582.80 | 582.80 | 671.72 |
| crystal size/mm | 0.5 × 0.48 × 0.33 | 0.28 × 0.06 × 0.02 | 0.31 × 0.08 × 0.03 | 0.19 × 0.10 × 0.04 | 0.46 × 0.05 × 0.03 |
| 2$\theta$ range/deg | 6.806 − 46.952 | 2.40 − 54.00 | 4.10 − 54.00 | 4.20 − 54.00 | 3.10 − 54.00 |
| $h$; $k$; $l$; range | ±10; ± 12; ± 21 | ±10; ± 12; ± 21 | −9, 12; −12, 8; −14, 32 | −12, 11; ± 13; −23. 33 | ±12; −13, 11; −29, 33 |
| crystal system | monoclinic | monoclinic | orthorhombic | orthorhombic | orthorhombic |
| space group | $P2_1$ | $P2_1$ | $P2_12_12_1$ | $P2_12_12_1$ | $P2_12_12_1$ |
| $a$/Å | 8.244(5) | 8.1814(2) | 9.8239(14) | 9.859(2) | 10.064(2) |
| $b$/Å | 10.010(6) | 9.9745(2) | 10.4309(16) | 10.464(2) | 10.522(2) |
| $c$/Å | 17.064(10) | 17.0287(4) | 26.433(4) | 26.470(5) | 26.340(5) |
| $\beta$/deg | 90.974(10) | 90.810(2) | 90 | 90 | 90 |
| $V$/Å$^3$ | 1408.0(15) | 1389.49(5) | 2708.6(7) | 2730.7(10) | 2789.4(10) |
| $Z$ | 2 | 2 | 4 | 4 | 4 |
| $D_{calc}$/g cm$^{-3}$ | 1.354 | 1.372 | 1.429 | 1.418 | 1.600 |
| $F$ (000) | 600 | 600 | 1200 | 1200 | 1344 |
| $\mu$/mm$^{-1}$ | 0.912 | 0.924 | 1.134 | 1.125 | 3.775 |
| max/min transmission | 0.7530/0.6571 | 0.9863/0.7840 | 0.9657/0.7200 | 0.9574/0.8163 | 0.9115/0.2779 |
| reflect. collected ($R_{int}$) | 11494 (0.0452) | 34711 (0.0798) | 12402 (0.0427) | 12066 (0.0609) | 16969 (0.0482) |
| independent reflections | 5635 | 6077 | 5277 | 5936 | 5995 |
| obs. reflect. [$I > 2\sigma(I)$] | 3766 | 4647 | 4389 | 4265 | 4480 |
| parameters refined | 352 | 352 | 334 | 334 | 328 |
| max./min. $\Delta\rho^a$/e Å$^{-3}$ | 0.236/−0.298 | 0.220/−0.220 | 0.467/−0.492 | 0.486/−0.354 | 0.637/−0.531 |
| $R_1/wR_2$ [$I > 2\sigma(I)$] [b] | 0.0315/0.0566 | 0.0372/0.0650 | 0.0383/0.0719 | 0.0492/0.0851 | 0.0396/0.0646 |
| $R_1/wR_2$ (all reflect.) [b] | 0.0470/0.0587 | 0.0648/0.0725 | 0.0510/0.0754 | 0.0810/0.0952 | 0.0676/0.0705 |
| goodness-of-fit on $F^2$ [c] | 0.722 | 1.041 | 1.027 | 0.973 | 1.001 |
| weight. scheme $w$; $a/b$ [d] | 0.0197/0.0000 | 0.0253/0.0000 | 0.0234/0.0000 | 0.0203/0.0000 | 0.0141/0.0000 |
| Flack parameter [e] | 0.068(8) | 0.017(9) | −0.001(10) | 0.007(13) | 0.008(9) |

[a] Largest difference peak and hole. [b] $R_1 = \Sigma||F_o| - |F_c||/\Sigma|F_o|$; $wR_2 = [\Sigma w(F_o^2 - F_c^2)^2/\Sigma w(F_o^2)^2]^{1/2}$. [c] Goodness-of-fit = $[\Sigma[w(F_o^2 - F_c^2)^2]/(n-p)]^{1/2}$. [d] $w = 1/[\sigma^2(F_o^2) + (aP)^2 + bP]$ where $P = (\max(F_o^2 \text{ or } 0) + 2F_c^2)/3$. [e] Absolute structure parameter.[25]

H9, $J$ = 6.72). $^1$H NMR ($CD_3OD$, 200 MHz), $\delta$/ppm ($J$/Hz) = 8.54 (s, 1H, H7), 7.42−7.26 (m, 2H (H3, H5) and 4H (H11/11′, H12/12′), 6.91−6.83 (m, 2H, H2, H4), 4.61 (q, 1H, H8, $J$ = 6.5), 1.58 (d, 3H, H9, $J$ = 7.0). $^{13}$C NMR ($CDCl_3$, 400 MHz), $\delta$/ppm =163.7, 160.9, 142.3, 133.0, 132.4, 131.4, 129.5 (C7, C1, C10, C13, C5, C3, C6), 128.8 (C12, C12′), 127.7 (C11, C11′), 118.7, 117.0, 67.9, 24.9 (C4, C2, C8, C9). (see Scheme 3 for NMR atom numbering). $[\alpha]^{25}_{589}$ ($c$ = 11.8 mg/mL): −140.7°.

**(*R*)-*N*-(1-(4-bromophenyl)ethyl)salicylaldimine, *R*-3.** mp 74 °C. Yield: 6.77 g, 90%. $C_{15}H_{14}NOBr$ (304.19 g·mol$^{-1}$): calculated C 59.23, H 4.64, N 4.60; found C 59.41, H 4.34, N 4.47%. IR (cm$^{-1}$):3050.66 (w), 2972.86 (w), 2888.47 (w), 1900.74 (w), 1630.47 (s), 1577.11 (m), 1489.33 (m), 1452.00 (m), 1416.23 (w), 1401.97 (m), 1379.82 (m), 1315.23 (w), 1278.05 (s), 1220.65 (w), 1204.70 (m), 1149.68 (m), 1129.32 (m), 1109.48 (s), 1008.87 (s), 975.93 (s), 922.79 (s), 846.18 (s), 822.52 (s), 798.22 (m), 757.29 (s), 716.47 (m), 645.87 (m), 621.64 (w), 523.38 (s), 474.17 (m), 455.76 (w). $^1$H NMR ($CD_3OD$, 200 MHz), $\delta$/ppm ($J$/Hz) = 8.54 (s, 1H, H7), 7.50 ("d", 2H, H12/12′, $J$ = 8.6), 7.38−7.25 (m, 2H, H3, H5), 7.32 ("d", 2H, H11/11′, $J$ = 8.4), 6.92−6.84 (m, 2H, H2, H4), 4.59 (q, 1H, H8, $J$ = 6.7), 1.58 (d, 3H, H9, $J$ = 6.2) (see Scheme 3 for NMR atom numbering). $[\alpha]^{25}_{589}$ ($c$ = 11.1 mg/mL): −122.0°.

**Δ/Λ-bis{(*R*)- or (*S*)-*N*-(1-(4-*X*-phenyl)ethyl)salicylaldiminato-$\kappa^2$*N*,*O*}zinc(II).** *General Procedure.* A methanolic solution (10 mL) of (*R*)-*N*-(1-(4-*X*-phenyl)ethyl)salicylaldimine [2-((*R*)-(1-(4-*X*)ethylimino)-methyl)phenol] (0.26 g, 1.0 mmol) was added to a methanolic solution (5 mL) of zinc(II) nitrate hexahydrate (0.15 g, 0.5 mmol) and to this was added triethylamin (140 $\mu$L). The mixture was refluxed for 1 h and filtered. Slow solvent evaporation from the filtrate gave colorless to light-yellow crystals after a few days. Analytical results are summarized in Table 4.

The IR spectra of the metal complexes show the characteristic absorption attributed to the $\nu$-(C═N) vibration around 1615 cm$^{-1}$ as described in similar complexes.[53]

**Δ/Λ-bis{(*R*)-N-(1-(4-methoxyphenyl)ethyl)salicylaldiminato-$\kappa^2$N,O}zinc(II), Δ/Λ-Zn-*R*-1.** $^1$H NMR ($CDCl_3$, 400 MHz), $\delta$/ppm ($J$/Hz) of Λ-species = 7.96 (s, 1H, H7), 7.30 (dd, 1H, H3, $J$ = 8.88, 7.75), 7.02 (d, 1H, H5, $J$ = 7.75), 6.85 (d, 2H, H 12/12′, $J$ = 8.36), 6.82 (d, 1H, H2, $J$ = 7.8), 6.58 (dd, 1H, H4, $J$ = 9.0, 7.66), 6.57 (d, 2H, H 11/11′, $J$ = 8.45), 4.23 (q, 1H, H8, $J$ = 6.79), 3.73 (s, 3H, $OCH_3$); 1.45 (d, 3H, H9, $J$ = 6.81); $\delta$/ppm of Δ-species = 8.12 (s, 1H, H7), 7.18 (2H), 6.77 (3H), 4.55 (q, 1H, H8), 3.75 (s, 3H, $OCH_3$). (see Scheme 3 for atom numbering).

**Δ/Λ-bis{(*R*)-*N*-(1-(4-chlorophenyl)ethyl)salicylaldiminato-$\kappa^2$*N*,*O*}zinc(II), Δ/Λ-Zn-*R*-2.** $^1$H NMR ($CDCl_3$, 400 MHz), $\delta$/ppm ($J$/Hz) of Λ-species = 8.03 (s, 1H, H7), 7.34 (dd, 1H, H3, $J$ = 8.75, 7.62), 7.09 (d, 1H, H5, $J$ = 7.58), 6.97 (d, 2H, H 12/12′, $J$ = 8.08), 6.84 (d, 1H, H2, $J$ = 7.56), 6.81 (d, 2H, H 11/11′, $J$ = 8.14), 6.64 (dd, 1H, H4, $J$ = 8.75, 7.43), 4.21 (q, 1H, H8, $J$ = 6.86), 1.51 (d, 3H, H9, $J$ = 6.86); $\delta$/ppm of Δ-species = 8.15 (s, 1H, H7), 7.22 (m, 4H), 7.03 (d, 1H), 6.58 (dd, 1H), 4.57 (q, 1H, H8). $^{13}$C NMR ($CDCl_3$, 400 MHz), $\delta$/ppm = 170.3, 168.9, 138.7, 135.8, 135.3, 133.6 (C1, C7, C10, C5, C3, C13), 129.0 (C11, C11′), 128.7 (C12, C12′), 123.2, 118.1, 114.6, 69.1, 22.1 (C2, C6, C4, C8, C9) (see Scheme 3 for atom numbering).

**Λ-bis{(*R*)-N-(1-(4-bromophenyl)ethyl)salicylaldiminato-$\kappa^2$N,O}zinc(II), Λ-Zn-*R*-3.** $^1$H NMR ($CDCl_3$, 400 MHz), $\delta$/ppm

(*J*/Hz) of Λ-species = 8.03 (s, 1H, H7), 7.34 (dd, 1H, H3, *J* = 8.81, 8.45), 7.12 (d, 2H, H 12/12′, *J* = 8.34), 7.09 (d, 1H, H5, *J* = 7.0), 6.84 (d, 1H, H2, *J* = 8.47), 6.75 (d, 2H, H 11/11′, *J* = 8.25), 6.64 (dd, 1H, H4, *J* = 8.82, 7.31), 4.20 (q, 1H, H8, *J* = 6.69), 1.51 (d, 3H, H9, *J* = 6.80); δ/ppm of Δ-species = 8.15 (s, 1H, H7), 7.16 (4H), 7.04 (1H), 6.58 (1H), 4.54 (q, 1H, H8). (see Scheme 3 for atom numbering).

**X-ray Crystallography.** Single-crystal X-ray structural analysis is a direct method to determine the absolute configuration of a chiral molecule using diffraction intensity differences due to anomalous X-ray scattering or dispersion in the presence of a "heavy atom" with the Bijvoet or related methods.[24] The distinction of inversion-related models of a noncentrosymmetric crystal structure is measured by the Flack parameter.[25] Suitable single crystals were carefully selected under a polarizing microscope. *Data Collection:* Bruker AXS with APEXII CCD area-detector, Mo−Kα radiation (λ = 0.71073 Å), temperature 203(2) K, graphite monochromator, double-pass method ω-scan, Data collection and cell refinement with APEX2,[54] respectively, cell refinement and data reduction with SAINT,[54] experimental absorption correction with SADABS.[55] *Structure Analysis and Refinement*: The structure was solved by direct methods (SHELXS-97);[56] refinement was done by full-matrix least-squares on $F^2$ using the SHELXL-97 program suite.[56] All non-hydrogen positions were refined with anisotropic temperature factors. Hydrogen atoms on carbon were positioned geometrically (C−H = 0.99 Å for aliphatic CH, C−H = 0.97 Å for $CH_3$, 0.94 Å for aromatic CH) and refined using a riding model (AFIX 13, 33, 43, respectively), with $U_{iso}(H) = 1.2U_{eq}(CH)$ and $1.5U_{eq}(CH_3)$.

Graphics were obtained with DIAMOND.[39] Crystal data and details on the structure refinement are given in Table 5. The structural data has been deposited with the Cambridge Crystallographic Data Center (CCDC-numbers 841950−841954).

**VCD Measurements.** $CDCl_3$ solution samples were placed in a 100 μm path length $BaF_2$ cell. IR and VCD spectra of 26 mM solutions of Zn-*R*-**2**, Zn-*S*-**2** and Zn-*R*-**3** were recorded on a Chira*IR* Dual-PEM VCD spectrometer from BioTools with 4 $cm^{-1}$ resolution. The spectra represent the average of a 4-h measurement. For 4 $cm^{-1}$ resolution VCD spectra of Zn-*R*-**1** (26 mM) and *R*-**2** (66 mM) we employed a Bruker Tensor 27 FTIR spectrometer equipped with the Bruker PMA 50 VCD sidebench module, using a data collection time of 6 h. All spectra were corrected for background effects by solvent subtraction. For VCD measurements between 1800 and 800 $cm^{-1}$, the optimum retardation value of the photoelastic modulator (PEM) used for the high-frequency circular polarization modulation of the FT-IR beam was set near the middle of the spectral range at 1400 $cm^{-1}$.

**Quantum-Chemical Calculations.** A rough estimate for the number and the geometries of conformer models for each diastereomer (Δ-Zn-*R*-2 and Λ-Zn-*R*-2) was obtained by applying the MMFF level conformer search from SPARTAN (Wave function Inc., Irvine, CA). These conformers were geometry optimized at the DFT level in GAUSSIAN[46] using the B3LYP functional with the 6-31G(d) basis set for C, O, H, N, and Cl and Ahlrichs VTZ[45] for zinc which resulted into three unique conformers each for Δ and Λ. Two low-energy conformers of Λ and one low-energy conformer of Δ were chosen for calculation of vibrational frequencies, IR/VCD intensities, relative energies (Δ*E*), and relative free energies (Δ*G*) at the B3LYP level using Ahlrichs VTZ for Zn and using 6-31+G(d,p), which adds an additional polarization function on H and a diffuse function on C, O, H, N, and Cl (GAUSSIAN). Frequencies were scaled by 0.97 for IR/VCD spectra and for the calculation of thermochemical parameters. Thermochemical parameters were corrected for internal rotations using the hindered rotor algorithm in GAUSSIAN. Theoretical spectra were constructed from calculated intensities simulating bands for each IR or VCD intensity using a Lorentzian function with a bandwidth of 6 $cm^{-1}$.

## ■ ASSOCIATED CONTENT

**Supporting Information.** Crystal photographs, additional molecular structure figures, details of 2D-NMR studies, geometries of modeled conformers, CIF files reported in this paper. This material is available free of charge via the Internet at http://pubs.acs.org.

## ■ AUTHOR INFORMATION

### Corresponding Author

*E-mail: steffen.luedeke@pharmazie.uni-freiburg.de (S.L.), janiak@uni-duesseldorf.de (C.J.).

### Present Addresses

⊥Institut für Anorganische Chemie und Strukturchemie, Universität Düsseldorf, Universitätsstrasse 1, D-40225 Düsseldorf, Germany.

## ■ ACKNOWLEDGMENT

We thank Dr. Klaus Ditrich (ChiPros) at BASF AG, Ludwigshafen, for providing the enantiopure (*R*)- or (*S*)-*N*-(4-*X*-phenyl)ethylamines. We acknowledge the financial support DFG-grant Ja466/14-1. Mr. Robin Brückner is thanked for his help in some of the synthetic work. We would like to acknowledge the use of the computing resources provided by the Black Forest Grid Initiative.

## ■ DEDICATION

Dedicated to Prof. Henri Brunner on the occasion of his 75th birthday.

## ■ REFERENCES

(1) Nozaki, H.; Moriuti, S.; Takaya, H.; Noyori, R. *Tetrahedron Lett.* **1966**, *7*, 5239–5244.

(2) (a) Amouri, H.; Gruselle, M. *Chirality in Transition Metal Chemistry*; Wiley: Chichester, 2008. (b) von Zelewsky, A. *Stereochemistry of Coordination Compounds*; Wiley: Chichester, 1995.

(3) (a) Kongprakaiwoot, N.; Armstrong, J. B.; Noll, B. C.; Brown, S. N. *Dalton Trans.* **2010**, *39*, 10105–10115. (b) Lv, W.; Zhu, P.-H.; Bian, Y.-Z.; Ma, C.-Q.; Zhang, X.-M.; Jiang, J.-Z. *Inorg. Chem.* **2010**, *49*, 6628–6635. (c) Ignatieva, S. N.; Balueva, A. S.; Karasik, A. A.; Latypov, S. K.; Nikonova, A. G.; Naumova, O. E.; Lonnecke, P.; Hey-Hawkins, E.; Sinyashin, O. G. *Inorg. Chem.* **2010**, *49*, 5407–5412. (d) Kanao, K.; Tanabe, Y.; Miyake, Y.; Nishibayashi, Y. *Organometallics* **2010**, *29*, 2381–2384. (e) Scholten, U.; Diserens, C.; Stoeckli-Evans, H.; Bernauer, K.; Meyer, M.; Stuppfler, L.; Lucas, D. *Inorg. Chem.* **2009**, *48*, 10942–10953. (f) Farber, C.; Wolmershauser, G.; Sitzmann, H. Z. *Z. Naturforsch.* **2009**, *64*, 25–40.

(4) (a) Brunner, H.; Tsuno, T. *Acc. Chem. Res.* **2009**, *42*, 1501–1510. (b) Brunner, H.; Muschiol, M.; Tsuno, T.; Takahashi, T.; Zabel, M. *Organometallics* **2008**, *27*, 3514–3525. (c) Brunner, H.; Zwack, T.; Zabel, M. *Organometallics* **2003**, *22*, 1741–1750. (d) Brunner, H. *Eur. J. Inorg. Chem.* **2001**, 905–912.

(5) Von Zelewsky, A.; Mamula, O. J. *Chem. Soc., Dalton Trans.* **2000**, 219–231.

(6) (a) Constable, E. C.; Zhang, G.; Housecroft, C. E.; Neuburger, M.; Zampese, J. A. *Chem. Commun.* **2010**, 3077–3079. (b) Constable, E. C.; Housecroft, C. E.; Kulke, T.; Lazzarini, C.; Schofield, E. R.; Zimmermann, Y. *J. Chem. Soc., Dalton Trans.* **2001**, 2864–2871.

(7) Piper, T. S. *J. Am. Chem. Soc.* **1961**, *83*, 3908–3909.

(8) Sakiyama, H.; Ōkawa, H.; Matsumoto, N.; Kida, S. *Bull. Chem. Soc. Jpn.* **1991**, *64*, 2644–2647.

(9) Sakiyama, H.; Ōkawa, H.; Matsumoto, N.; Kida, S. *J. Chem. Soc., Dalton Trans.* **1990**, 2935–2939.
(10) Ernst, R. E.; ÓConnor, M. J.; Holm, R. H. *J. Am. Chem. Soc.* **1967**, *89*, 6104–6113.
(11) (a) Clegg, W.; Harrington, R. W.; North, M.; Pasquale, R. *Chem.—Eur. J.* **2010**, *16*, 6828–6843. (b) Escudero-Adán, E. C.; Martínez Belmonte, M.; Benet-Buchholz, J.; Kleij, A. W. *Org. Lett.* **2010**, *12*, 4592–4595. (c) Shibasaki, M.; Kanai, M.; Matsunaga, S.; Kumagai, N. *Acc. Chem. Res.* **2009**, *42*, 1117–1127. (d) Adao, P.; Pessoa, J. C.; Henriques, R. T.; Kuznetsov, M. L.; Avecilla, F.; Maurya, M. R.; Kumar, U.; Correia, I. *Inorg. Chem.* **2009**, *48*, 3542–3561. (e) Niemeyer, J.; Kehr, G.; Fröhlich, R.; Erker, G. *Dalton Trans.* **2009**, 3731–3741. (f) Xu, Z.-X.; Huang, Z.-T.; Chen, C.-F. *Tetrahedron Lett.* **2009**, *50*, 5430–5433. (g) Lee, J.-J.; Yang, F.-Z.; Lin, Y.-F.; Chang, Y.-C.; Yu, K.-H.; Chang, M.-C.; Lee, G.-H.; Liu, Y.-H.; Wang, Y.; Liu, S.-T.; Chen, J.-T. *Dalton Trans.* **2008**, 5945–5956. (h) Jain, K. R.; Herrmann, W. A.; Kühn, F. E. *Coord. Chem. Rev.* **2008**, *252*, 556–568. (i) Chu, Z.; Huang, W.; Wang, L.; Gou, S. *Polyhedron* **2008**, *27*, 1079–1092. (j) Koth, D.; Gottschaldt, M.; Görls, H.; Pohle, K. *Beilstein J. Org. Chem.* **2006**, *2*, article 17 (DOI: 10.1186/1860-5397-2-17). (k) Cohen, C. T.; Chu, T.; Coates, G. W. *J. Am. Chem. Soc.* **2005**, *127*, 10869–10878. (l) Santoni, G.; Rehder, D. *J. Inorg. Biochem.* **2004**, *98*, 758–764. (m) Cozzi, P. G. *Chem. Soc. Rev.* **2004**, *33*, 410–421. (n) Larrow, J. F.; Jacobsen, E. N. *Top. Organomet. Chem.* **2004**, *6*, 123–152. (o) Sammis, G. M.; Danjo, H.; Jacobsen, E. N. *J. Am. Chem. Soc.* **2004**, *126*, 9928–9929. (p) Zhou, X. G.; Zhao, J.; Santos, A. M.; Kühn, F. E. *Z. Naturforsch.* **2004**, *59b*, 1223–122. (q) Dreos, R.; Nardin, G.; Randaccio, L.; Siega, P.; Tauzher, G. *Inorg. Chem.* **2004**, *43*, 3433–3440. (r) Gröger, H. *Chem. Rev.* **2003**, *103*, 2795–2828. (s) Sammis, G. M.; Jacobsen, E. N. *J. Am. Chem. Soc.* **2003**, *125*, 4442–4443. (t) Che, C.-M.; Huang, J.-S. *Coord. Chem. Rev.* **2003**, *242*, 97–113. (u) Larionov, O. V.; Savel'eva, T. F.; Kochetkov, K. A.; Ikonnokov, N. S.; Kozhushkov, S. I.; Yufit, D. S.; Howard, J. A. K.; Khrustalev, V. N.; Belokon, Y. N.; de Meijere, A. *Eur. J. Org. Chem.* **2003**, 869–877.
(12) Reviews: (a) Matsumoto, K.; Saito, B.; Katsuki, T. *Chem. Commun.* **2007**, 3619–3627. (b) Gupta, K. C.; Sutar, A. K. *Coord. Chem. Rev.* **2008**, *252*, 1420–1450. (c) Abdi, S. H. R.; Kureshy, R. I.; Khan, N. H.; Mayani, V. J.; Bajaj, H. C. *Catal. Surv. Asia* **2009**, *13*, 104–131. (d) Gupta, K. C.; Sutara, A. K.; Lin, C.-C. *Coord. Chem. Rev.* **2009**, *253*, 1926–1946. (e) Zulauf, A.; Mellah, M.; Hong, X.; Schulz, E. *Dalton Trans.* **2010**, *39*, 6911–6935. (f) Lin, L.-L.; Liu, X.-H.; Feng, X.-M. *Progr. Chem.* **2010**, *22*, 1353–1361.
(13) Evans, C.; Luneau, D. J. *Chem. Soc., Dalton Trans.* **2002**, 83–86; Zn(SB*)2 complexes with Λ-M-R-L configuration.
(14) Fan, L.-L.; Guo, F.-S.; Yun, L.; Lin, Z.-J.; Herchel, R.; Leng, J.-D.; Ou, Y.-C.; Tong, M.-L. *Dalton Trans.* **2010**, *39*, 1771–1780.
(15) Dhara, K.; Sarkar, K.; Roy, P.; Nandi, M.; Bhaumik, A.; Banerjee, P. *Tetrahedron* **2008**, *64*, 3153–3159.
(16) Yuan, G.; Zhu, C.; Xuan, W.; Cui, Y. *Chem.—Eur. J.* **2009**, *15*, 6428–6434.
(17) Xiao, J. M.; Zhang, W. *Inorg. Chem. Commun.* **2009**, *12*, 1175–1178.
(18) Howson, S. E.; Allan, L. E. N.; Chmel, N. P.; Clarkson, G. J.; van Gorkum, R.; Scott, P. *Chem. Commun.* **2009**, 1727–1729.
(19) Becker, J. M.; Barker, J.; Clarkson, G. J.; van Gorkum, R.; Johal, G. K.; Walton, R. I.; Scott, P. *Dalton Trans.* **2010**, *39*, 2309–2326.
(20) Tapiero, H.; Tew, K. D. *Biomed. Pharmacother.* **2003**, *57*, 399–411.
(21) Lipscomb, W. N.; Strater, N. *Chem. Rev.* **1996**, *96*, 2375–2434.
(22) Dudev, T.; Lim, C. *J. Am. Chem. Soc.* **2000**, *122*, 11146–11153.
(23) Li, Z.; Liu, G.; Zheng, Z.; Cheng, H. *Tetrahedron* **2000**, *56*, 7187–7191.
(24) Paulus, E. F.; Gieren, A. Structure analysis by diffraction. In *Handbook of analytical techniques*; Günzler, H., Williams, A., Eds.; Wiley-VCH: New York, 2001; Vol. 1.
(25) (a) Flack, H. D.; Sadki, M.; Thompson, A. L.; Watkin, D. J. *Acta Crystallogr., Sect. A* **2011**, *67*, 21–34. (b) Flack, H. D.; Bernardinelli, G. *Chirality* **2008**, *20*, 681–690. (c) Flack, H. D.; Bernardinelli, G. *Acta Crystallogr., Sect. A* **1999**, *55*, 908–915. (d) Flack, H. D. *Acta Crystallogr., Sect. A* **1983**, *39*, 876–881.
(26) Berova, N.; Nakanishi, K.; Woody, R. W. *Circular Dichroism: Principles and Applications*, 2nd ed.; Wiley-VCH: New York, 2000.
(27) Bosnich, B. *J. Am. Chem. Soc.* **1968**, *90*, 627–632.
(28) Clark-Baldwin, K.; Tierney, D. L.; Govindaswamy, N.; Gruff, E. S.; Kim, C.; Berg, J.; Koch, S. A.; Penner-Hahn, J. E. *J. Am. Chem. Soc.* **1998**, *120*, 8401–8409.
(29) Seitz, M.; Stempfhuber, S.; Zabel, M.; Schütz, M.; Reiser, O. *Angew. Chem., Int. Ed.* **2005**, *44*, 242–245.
(30) Nafie, L. A. *Nat. Prod. Commun.* **2008**, *3*, 451–466.
(31) Stephens, P. J.; Devlin, F. J.; Pan, J.-J. *Chirality* **2008**, *20*, 643–663.
(32) Freedman, T. B.; Cao, X. L.; Young, D. A.; Nafie, L. A. *J. Phys. Chem. A* **2002**, *106*, 3560–3565.
(33) He, Y. N.; Cao, X. L.; Nafie, L. A.; Freedman, T. B. *J. Am. Chem. Soc.* **2001**, *123*, 11320–11321.
(34) Sato, H.; Mori, Y.; Fukuda, Y.; Yamagishi, A. *Inorg. Chem.* **2009**, *48*, 4354–4361.
(35) (a) Gil-Hernández, B.; Höppe, H.; Vieth, J. K.; Sanchiz, J.; Janiak, C. *Chem. Commun.* **2010**, *46*, 8270–8272. (b) Janiak, C.; Chamayou, A.-C.; Uddin, A. K. M. R.; Uddin, M.; Hagen, K. S.; Enamullah, M. *Dalton Trans.* **2009**, 3698–3709. (c) Flack, H. D. *Acta Crystallogr., Sect. A* **2009**, *65*, 371–389. (d) Enamullah, M.; Sharmin, A.; Hasegawa, M.; Hoshi, T.; Chamayou, A.-C.; Janiak, C. *Eur. J. Inorg. Chem.* **2006**, 2146–2154.
(36) Shibuya, Y.; Nabari, K.; Kondo, M.; Yasue, S.; Maeda, K.; Uchida, F.; Kawaguchi, H. *Chem. Lett.* **2008**, *37*, 78–79.
(37) Yang, L.; Powell, D. R.; Houser, R. P. *Dalton Trans.* **2007**, 955–964.
(38) Addison, A. W.; Rao, T. N.; Reedijk, J.; van Rijn, J.; Verschoor, G. C. *J. Chem. Soc., Dalton Trans.* **1984**, 1349–1356.
(39) Brandenburg, K. *Diamond, Crystal and Molecular Structure Visualization*, Version 3.2; Crystal Impact—K. Brandenburg & H. Putz Gbr: Bonn, Germany, 2009.
(40) Orpen, A. G.; Brammer, L.; Allen, F. H.; Kennard, O.; Watson, D. G.; Taylor, R. J. *Chem. Soc., Dalton Trans.* **1989**, Supplement 1.
(41) Related Co Schiff base complexes: Benisvy, L.; Bill, E.; Blake, A. J.; Collison, D.; Davies, E. S.; Garner, C. D.; Guindy, C. I.; McInnes, E. J. L.; McArdle, G.; McMaster, J.; Wilson, C.; Wolowska, J. *Dalton Trans.* **2004**, 3647–3653.
(42) (a) Calligaris, M.; G. Nardin, G.; Randaccio, L. *Coord. Chem. Rev.* **1972**, *7*, 385–403. (b) Cesari, M.; Neri, C.; Perego, G.; Perrotti, E.; Zazzetta, A. *Chem. Commun.* **1970**, 276–277.
(43) Related Cu Schiff base complexes: (a) Benisvy, L.; Blake, A. J.; Collison, D.; Davies, E. S.; Garner, C. D.; McInnes, E. J. L.; McMaster, J.; Whittaker, G.; Wilson, C. *Dalton Trans.* **2003**, 1975–1985. (b) Fernandez, J. M.; Ruíz-Ramírez, O. L.; Toscano, R. A.; Macías-Ruvalcaba, N.; Aguilar-Martínez, M. *Trans. Met. Chem.* **2000**, *25*, 511–517. (c) Elerman, Y.; Elmali, A.; Süheyla, O. *Acta Crystallogr.* **1998**, *C54*, 1072–1074. (d) Akitsu, T.; Einaga, Y. *Acta Crystallogr.* **2004**, *C60*, m640–m642. (e) Matsumoto, N.; Nonaka, Y.; Kida, S.; Kawano, S.; Ueda, I. *Inorg. Chim. Acta* **1979**, *37*, 27–36. (f) Cline, S. J.; Wasson., J. R.; Hatfield, W. E.; Hodgson, D. J. *J. Chem. Soc., Dalton Trans.* **1978**, 1051–1057. (g) Orioli, P. L.; Sacconi, L. *J. Am. Chem. Soc.* **1966**, *88*, 277–280.
(44) Related Zn Schiff base complexes: (a) Orioli, P. L.; Di Vaira, M.; Sacconi, L. *Chem. Commun.* **1965**, 103–103. (b) Orioli, P. L.; Di Vaira, M.; Sacconi, L. *Inorg. Chem.* **1966**, *5*, 400–405. (c) Hall, D.; Moore, F. H. *Proc. Chem. Soc.* **1960**, 256–256.
(45) Schäfer, A.; Horn, H.; Ahlrichs, R. *J. Chem. Phys.* **1992**, *97*, 2571–2577.
(46) Frisch, M. J., Trucks, G. W., Schlegel, H. B., Scuseria, G. E., Robb, M. A., Cheeseman, J. R., Scalmani, G., Barone, V., Mennucci, B., Petersson, G. A., Nakatsuji, H., Caricato, M., Li, X., Hratchian, H. P., Izmaylov, A. F., Bloino, J., Zheng, G., Sonnenberg, J. L., Hada, M., Ehara, M., Toyota, K., Fukuda, R., Hasegawa, J., Ishida, M., Nakajima, T., Honda, Y., Kitao, O., Nakai, H., Vreven, T., Montgomery, Jr., J. A., Peralta, J. E., Ogliaro, F., Bearpark, M., Heyd, J. J., Brothers, E., Kudin, K. N., Staroverov, V. N., Kobayashi, R., Normand, J., Raghavachari, K., Rendell, A., Burant, J. C., Iyengar, S. S., Tomasi, J., Cossi, M., Rega, N.,

Millam, N. J., Klene, M., Knox, J. E., Cross, J. B., Bakken, V., Adamo, C., Jaramillo, J., Gomperts, R., Stratmann, R. E., Yazyev, O., Austin, A. J., Cammi, R., Pomelli, C., Ochterski, J. W., Martin, R. L., Morokuma, K., Zakrzewski, V. G., Voth, G. A., Salvador, P., Dannenberg, J. J., Dapprich, S., Daniels, A. D., Farkas, Ö., Foresman, J. B., Ortiz, J. V., Cioslowski, J., Fox, D. J. *Gaussian 09*, Revision B.01; Gaussian, Inc.: Wallingford, CT, 2009.

(47) Allenmark, S. G. *Nat. Prod. Rep.* **2000**, *17*, 145–155.

(48) Harada, N.; Ono, H.; Uda, H.; Parveen, M.; Khan, N. U. D.; Achari, B.; Dutta, P. K. *J. Am. Chem. Soc.* **1992**, *114*, 7687–7692.

(49) Berova, N.; Nakanishi, K. Exciton Chirality Method: Principles and Applications. In *Circular Dichroism, Principles and Applications*, 2nd ed.; Berova, N., Nakanishi, K., Woody, R. W., Eds.; Wiley-VCH: New York, 2000; pp 337−382.

(50) Sato, H.; Taniguchi, T.; Nakahashi, A.; Monde, K.; Yamagishi, A. *Inorg. Chem.* **2007**, *46*, 6755–6766.

(51) Brunner, H.; Oeschey, R.; Nuber, B. *J. Chem. Soc., Dalton Trans.* **1996**, 1499–1508.

(52) Enamullah, M.; Royhan Uddin, A. K. M.; Chamayou, A. C.; Janiak, C. *Z. Naturforsch.* **2007**, *62b*, 807–81.

(53) Kovacic, J. E. *Spectrochim. Acta* **1967**, *23A*, 183–187.

(54) *APEX2, Data Collection Program for the CCD Area-Detector System*, Version 2.1−0; *SAINT, Data Reduction and Frame Integration Program for the CCD Area-Detector System*; Bruker Analytical X-ray Systems: Madison, WI, 2006.

(55) Sheldrick, G. *SADABS, Area-detector absorption correction*; University of Göttingen: Göttingen, Germany, 1996.

(56) Sheldrick, G. M. *Acta Crystallogr., Sect. A* **2008**, *64*, 112–122. Sheldrick, G. M. *SHELXS-97, SHELXL-97, Programs for Crystal Structure Analysis*; University of Göttingen: Göttingen, Germany, 1997.